On the Value of a Multistage Optimization Approach for Intensity-Modulated Radiation Therapy Planning*

D, Wood[1], S. Çetinkaya[†1,2], H. Gangammanavar[1], W. Lu[3], and J. Wang[3]

[1]Department of Operations Research and Engineering Management, SMU, Dallas, TX.
[2]Department of Internal Medicine, UTSW Medical Center, Dallas, TX.
[3]Department of Radiation Oncology, UTSW Medical Center, Dallas, TX.

Submitted to *Physics in Medicine and Biology*, February 3, 2022
Version: February 26, 2022

Abstract

The goal of intensity-modulated radiation therapy (IMRT) is to precisely distribute a prescribed dose of radiation to cancerous tumors while sparing the surrounding healthy tissue. A typical approach to IMRT planning uniformly divides and allocates the same dose prescription across several successive treatment sessions. This uniform prescription allocation scheme then couples with a static optimization-based model to identify the fluence map (FM), a.k.a., beamlet intensity profile. The resulting treatment plan then requires repeated delivery of the same FM for each treatment session without considering the patient's organ and tumor volume evolution over future treatment sessions. In this paper, we introduce a nonuniform generalization of the uniform allocation scheme that does not automatically assume equal session dose prescriptions. Instead, we identify optimal dose prescriptions and FMs for individual sessions via new multistage optimization-based models which are compared numerically in terms of multiple metrics and resulting dose-volume histograms (DVHs). Our numerical results show the restrictive nature of the uniform allocation scheme and demonstrate the value of nonuniform multistage models across multiple performance metrics including tumor delivery precision and healthy tissue exposure to radiation. These results make a case in support of employing multistage stochastic programming methodology to derive ideal allocation schemes and FMs simultaneously.

*This work has been conducted under a Lyle School (SMU) Interdisciplinary Research Seed Funding Grant and Radiation Oncology MAIA Lab (UTSW) Educational Experience Agreement (UTSW Contract ID # 2020-7031).
[†]Corresponding author: sila@smu.edu

1 Introduction and Relevant Literature

Radiation therapy is a common treatment method for various forms of cancer, and it involves meticulously exposing the impacted tissues to radiation to kill the malignant tumor cells. For successful treatment outcomes, it is key to deliver the prescribed radiation dose to the tumor while minimizing exposure to healthy organs-at-risk (OAR) [1, 2]. The common scheduling practice for radiation therapy treatment includes multiple successive sessions (*fractions*) occurring regularly over several weeks. This fragmented scheduling approach is known as a *fractionation scheme*. A fractionation scheme is advantageous because healthy cells can effectively repair sublethal damage between fractions whereas the tumor cells are much less capable [3]. As clinical imaging, delivery technologies, and computational capabilities have improved, there has been a continual need to study and improve the existing optimization-based radiation therapy planning (RTP) practices and approaches. In this paper, we revisit this need with a specific focus on Intensity-Modulated Radiation Therapy (IMRT), an advanced technology known to produce a precise and conformal radiation dosage delivery by utilizing numerous beamlets with varying intensities.

Since its first clinical implementation in 1994, IMRT has resulted in significant reductions of radiation exposure to healthy tissues for patients undergoing treatment [4, 5]. Effective delivery of IMRT relies on optimization-based RTP models and methodologies in order to obtain an optimal fluence map (FM), a.k.a., beamlet intensity profile. The FM is determined while considering the state of the patient (volume of the tumor and its position relative to OARs as seen on volumetric imaging such as a CT scan) and the tumor prescription provided by a clinician [6, 7, 8, 9, 10, 11, 12, 13, 14, 15]. For detailed reviews of optimization-based approaches for IMRT, we refer to [6, 9, 13], and here we focus on and cite the previous work that is most closely related to the current paper.

A popular optimization-based approach for determining the optimal FM is through the implementation of RTP models with a least-squares objective function. RTP models that incorporate a least-squares objective function date back several decades [10, 11, 14] and we refer to Section

2.3.1 of [9] for a review of this class of RTP optimization models. A least-squares objective, in the context of an RTP problem, penalizes any deviation between the given prescription and the radiation quantities delivered to the tumor. The resulting model will also typically include upper bound constraints on the amount of radiation exposure to surrounding OAR. Such current least-squares models determine the FM while only considering the patient's state at the beginning of radiation therapy, and the same FM is adopted for radiation delivery for all fractions to follow [16, 17]. We classify such an approach to RTP as the *static approach*.

The static approach assumes that the tumor prescription quantity and OAR upper bounds remain fixed and uniform across all fractions. We refer to this kind of a dose prescription allocation scheme as *uniform fractionation* in the remainder of this paper. However, with treatment lasting several weeks, the tumor and OAR structures are expected to reveal consistent **evolution** in volume between fractions [18, 19, 20]. A more flexible fractionation scheme would lend capability and perhaps allow the clinician to utilize updated CT scans or future predictions during the treatment process to make adjustments to treatment delivery. Therefore, there is a need to develop optimization-based models and methodologies that take advantage of this capability.

To this end, we propose RTP models and methodology that explicitly adapt the FM at each fraction in accordance with a patient's predicted structural volume evolution over time. The outcome is a multistage approach (in contrast to the existing static approach) and counterpart optimization-based models and methodologies that lend themselves to nonuniform (in contrast to the existing uniform) fractionation schemes. A CT scan provides essential information only at the current point in time. However, the radiation delivered in a given fraction impacts the future evolution of the tumor and surrounding structures. Hence, our proposed multistage approach with a nonuniform fractionation scheme is more amenable to incorporate **uncertainty in regards to evolution of the tumor and OAR over future fractions** (a.k.a., *interfractional uncertainty* [17]) and adapt FMs in response to uncertainty.

Ultimately, our paper aims to enhance and inform the existing optimization-based practice for RTP to include a stochastic multistage framework. Hence, we systematically examine potential shortcomings of the static approach compared to the proposed multistage approach. To this end,

we explore the value of a *nonuniform fractionation* scheme and illustrate that allowing the dose prescriptions to vary across fractions may have quantifiable advantages worthy of evaluation by clinical experts. First, we assume a deterministic setting (with perfect tumor evolution predictions for each fraction). We offer computational results using prostate cancer patient CT scan data and provide comparison across various metrics of interest and resulting dose-volume histograms (DVHs). We also explore potential insights from models that restrict the degree of nonuniformity in the fractionation scheme. Next, we consider the more realistic stochastic case with interfractional uncertainty and present comprehensive results obtained by utilizing scenario trees where each node represents a different CT scan prediction.

By implementing stochastic programming methodology for multistage RTP models with interfractional uncertainty, we provide a proof-of-concept justifying the importance of modeling stochasticity using predictive analytics tools. Thereby, we make a case in support of employing multistage stochastic programming methodology to derive ideal allocation schemes and beam profile solutions, simultaneously, in contrast to the common practice static approach.

The rest of the paper is organized as follows. In Section 2, we present the notation and foundational elements of the optimization-based RTP models investigated in the paper. We also present the main performance metrics used to compare the different approaches for RTP. In Section 3, we consider a deterministic multistage setting as a building block of the proposed stochastic multistage formulations and demonstrate the value of our proposed nonuniform fractionation scheme. In Section 4, we extend the deterministic case to explicitly take into account interfractional uncertainty. Next, in Section 4.3, we provide a comparative analysis of the performance and demonstrate the potential benefits of the stochastic multistage models in a three-stage RTP experiment. Finally, we present a summary of our results and conclusions in Section 5.

2 Fundamentals of Optimization-Based Modeling for RTP

We begin with introducing fundamental notions of the optimization-based IMRT planning problems at hand along with the corresponding notation adopted throughout this paper. In terms of the notation, let us first note that we use boldface lowercase letters when referring to a vector

(e.g., $\mathbf{z}_n$), boldface uppercase letters for a matrix (e.g., $\mathbf{A}_n$), and calligraphic uppercase letters (e.g., $\mathcal{O}$) for sets. Also, we reserve the assignment of subscripts for the purposes of time or stage indices, and we note that $[a]_+ := \max\{a, 0\}$ and $[a]_- := \max\{-a, 0\}$ for $a \in \mathbb{R}$. For a summary of all essential notation used throughout this paper, we refer to Appendix A.

2.1 Problem Definition, Modeling Assumptions, and Notation

Suppose we have a fractionation scheme comprising of N fractions. At the beginning of any fraction, we have the ability to obtain a CT scan which captures a 3D representation of the patient's current state (structural volumes and positions) and includes all relevant structures such as the tumor, the nearby OARs, and normal body tissue. We collectively denote these structures by $\mathcal{T}$. Depending on the type and location of cancer, the set of OAR, denoted as $\mathcal{O} \subset \mathcal{T}$, is different. For example, the CT scan of a prostate cancer patient may have an OAR set given by $\mathcal{O} := \{\text{rectum, bladder, left femur, right femur}\}$.

We emphasize the idea that each CT scan represents an instantaneous observation of the patient's state (denoted ξ_n in fraction n) and can be viewed as a realization of a stochastic process $\{\tilde{\xi}\}$ associated with the evolution of a patient's structures. For clarity, a distinction is made when a particular CT scan observation is currently known (ξ_n) (has already been realized/obtained) or currently unknown ($\tilde{\xi}_n$) (to be revealed in the future). The information in a CT scan is discretized into a three-dimensional grid, where the smallest unit is called a *voxel*. Based on its relative position, a voxel (v) is classified as belonging to a specific structure $i \in \mathcal{T}$. We use $\mathcal{V}_n^{(i)}$ to represent the set of voxels in a particular fraction n classified to structure $i \in \mathcal{T}$. We define the set of all voxels as $\mathcal{V}_n := \bigcup_{i \in \mathcal{T}} \mathcal{V}_n^{(i)}$.

The fractionation scheme takes the *dose prescription* as an input which dictates the total quantity of radiation (in Gray (Gy) units) assigned for delivery to the patient's tumor (L^{tumor}) across all N fractions. The does prescription also dictates structure specific upper bounds, denoted by the vector $\mathbf{u}$, on the amount of radiation delivered to the surrounding OAR. The total quantity of radiation is distributed into fraction-specific prescription quantities captured by variables ℓ_n and $\mathbf{z}_n$ for tumor and OAR, respectively, in a given fraction n, respectively.

That is, ℓ_n is the radiation amount assigned for delivery to the tumor whereas $\mathbf{z}_n$ is the upper bound on the amount of radiation delivered to OAR in fraction n. Therefore, the decision vector $(\mathbf{z}_n, \ell_n)$ specifies the fraction-specific dose prescriptions. Clearly, these variables must satisfy

$$\sum_{n=1}^{N} \ell_n = L^{\text{tumor}}, \tag{DP.a}$$

$$\sum_{n=1}^{N} z_n^{(i)} \leq u^{(i)}, \quad i \in \mathcal{O}. \tag{DP.b}$$

Here, the first condition ensures that the sum of fraction-specific tumor dose prescriptions must be equal to the overall treatment dose prescription (L^{tumor}). The second condition limits the total of the OAR upper bounds for each structure $i \in \mathcal{O}$ to be at most the prescribed value given in $\mathbf{u}$.

To model the requirements of a fractionation scheme (uniform or nonuniform), we introduce a set of feasible fraction-specific dose prescriptions as

$$\mathcal{U}_n^{\epsilon} = \left\{ (\mathbf{z}_n, \ell_n) \;\middle|\; \begin{array}{ll} \dfrac{L^{\text{tumor}}}{N} \cdot (1-\epsilon) \leq \ell_n \leq \dfrac{L^{\text{tumor}}}{N} \cdot (1+\epsilon), & \text{(2a)} \\ \dfrac{u^{(i)}}{N} \cdot (1-\epsilon) \leq z_n^{(i)} \leq \dfrac{u^{(i)}}{N} \cdot (1+\epsilon), \quad i \in \mathcal{O}, . & \text{(2b)} \end{array} \right\}$$

Here, the parameter $\epsilon \geq 0$ determines the degree of nonuniformity allowed in choosing the fraction-specific prescription upper bounds. For instance, when $\epsilon = 0$, (2a) and (2b) imply a uniform fractionation scheme with tumor prescription $\ell_n = \frac{L^{\text{tumor}}}{N}$ and OAR upper bounds $z_n^{(i)} = \frac{u^{(i)}}{N}$ for structures $i \in \mathcal{O}$, for all fractions. On the other hand, we use $\mathcal{U}_n^M$ to imply a completely unrestricted nonuniform fractionation scheme, where M is a large positive scalar.

In a given fraction denoted by n, where $n = 1, \ldots, N$, a multileaf collimator is used to precisely conform radiation delivery to the tumor structure [2, 9, 21]. The radiation delivery involves determining the gantry angle (alignment of beams) and intensity of each individual beamlet. We denote the set of radiation beamlets as $\mathcal{B}$. We assume that the gantry angle is preselected and focus on determining the FM. For a given gantry angle and the information provided in a CT scan (ξ_n), a *dose-deposition matrix* that translates a given FM to the amount of radiation delivered to each individual voxel is computed. We denote the dose-deposition matrix in fraction n by $\mathbf{A}_n(\xi_n)$ to explicitly show its dependence on the CT-scan information.

An element a_{vbn} of the dose-deposition matrix $\mathbf{A}_n(\xi_n)$ captures the amount of radiation from beamlet $b \in \mathcal{B}$ delivered to voxel $v \in \mathcal{V}$. We denote the amount of radiation delivered to voxel $v \in \mathcal{V}$ by x_{vn}. If y_{bn} denotes the beamlet intensity for $b \in \mathcal{B}$, then we have $x_{vn} = \sum_{b \in \mathcal{B}} a_{vbn} y_{bn}$. This relationship can be written concisely as

$$\mathbf{x}_n = \mathbf{A}_n(\xi_n)\mathbf{y}_n \qquad \forall n = 1, \ldots, N. \tag{3}$$

The amount of radiation received by a OAR-classified voxel must be no more than the respective fraction-specific upper bound, that is

$$x_{vn} \leq z_n^{(i)} \qquad \forall v \in \mathcal{V}_n^{(i)},\ i \in \mathcal{O},\ n = 1, \ldots, N. \tag{4}$$

The optimization models presented in this paper simultaneously determine the distribution of the dose prescription into fraction-specific amounts and construct precise FMs for all fractions. The vector $(\mathbf{x}_n, \mathbf{y}_n)$ collectively determines the FM. The set of feasible fraction-specific radiation delivery decisions is then given by

$$\mathcal{S}_n(\xi_n) = \big\{(\mathbf{x}_n, \mathbf{y}_n, \mathbf{z}_n, \ell_n) \mid (3), (4),\ \mathbf{x}_n, \mathbf{y}_n, \mathbf{z}_n, \ell_n \geq 0\big\},\ n = 1, \ldots, N. \tag{5}$$

As previously mentioned, a popular method for meeting tumor dose prescription is through the use of a fraction-specific least-squares expression for

$$f_n(\mathbf{x}_n, \ell_n) = \sum_{v \in \mathcal{V}_n^{\text{tumor}}} \left[w_n^+ \Big(\big[x_{vn} - \ell_n \big]_+ \Big)^2 + w_n^- \Big(\big[x_{vn} - \ell_n \big]_- \Big)^2 \right],\ n = 1, \ldots, N. \tag{6}$$

Clearly, $f_n(\cdot)$ penalizes deviation between the quantity of radiation actually delivered to each voxel (x_{vn}) and the quantity prescribed in a given fraction (ℓ_n). In this sense, f_n is a measure of radiation delivery precision to all tumor voxels in a particular fraction ($\mathcal{V}_n^{\text{tumor}}$). The positive scalar weight parameters w_n^+ and w_n^- used in (6) reflect the preferences between overdosing and underdosing the tumor, respectively. For example, choosing a value $w_n^- > w_n^+$ implies heavier penalization to underdosing the tumor as opposed to overdosing the tumor. Without loss of generality, we use $w_n^+ + w_n^- = 1$ for $n = 1, \ldots, N$ in our numerical experiments.

2.2 Performance Evaluation Metrics

We next present the metrics useful to compare the performance of different optimization-based approaches of interest in this paper. These include the squared deviation penalty (SDP), over-

all total dose (TD-Overall), OAR total dose (TD-OAR), and tumor underdose (TUD). These metrics are are computed as

$$\text{SDP} = \sum_{n=1}^{N} f_n(\mathbf{x}_n, \ell_n), \qquad \text{TUD} = \frac{1}{N}\sum_{n=1}^{N} \frac{100 \times |\{v \in \mathcal{V}_n^{\text{tumor}} : x_{vn} < \ell_n\}|}{|\mathcal{V}_n^{\text{tumor}}|},$$

$$\text{TD-Overall} = \frac{\sum_{n=1}^{N}\sum_{i\in\mathcal{T}}\sum_{v\in\mathcal{V}_n^{(i)}} x_{vn}}{\sum_{n=1}^{N}\sum_{i\in\mathcal{T}}|\mathcal{V}_n^{(i)}|}, \qquad \text{and} \qquad \text{TD-OAR} = \frac{\sum_{n=1}^{N}\sum_{i\in\mathcal{O}}\sum_{v\in\mathcal{V}_n^{(i)}} x_{vn}}{\sum_{n=1}^{N}\sum_{i\in\mathcal{O}}|\mathcal{V}_n^{(i)}|},$$

where f_n is given in (6). SDP captures the total quadratic penalty on radiation delivery deviating from the dose prescription $(\ell_n)_{n=1}^N$. TD-Overall represents the average amount of radiation delivered to all voxels through the entire treatment horizon. This metric includes dosage delivered to all OAR, the tumor, and normal tissue. On the other hand, TD-OAR corresponds to the average amount of radiation delivered only to OAR voxels through the entire treatment horizon. TUD calculates the average percentage of tumor voxels that receive less than the prescribed amount of radiation. In addition to the metrics of interest above, we also define the notion of aggregate dose (AD) that represents the total amount of radiation delivered to all voxels through the entire treatment horizon. We compute this quantity as $\text{AD} = \sum_{n=1}^{N}\sum_{i\in\mathcal{T}}\sum_{v\in\mathcal{V}_n^{(i)}} x_{vn}$. We make references to this quantity whenever appropriate.

It is worthwhile to note that while the above metrics are fundamental for optimization-based approaches, they are not routinely evaluated for a clinical plan. Existing clinical routine evaluates a plan using DVHs. [1, 22]. Hence, we also present the comparison of our proposed models using DVHs.

2.3 Basic Model of the Static Approach

As we have noted earlier, standard practice for solving RTP problems is based on the static approach under which the treatment plan is designed and based only on the information ξ_1 revealed in the CT scan obtained before the commencement of the treatment. This approach provides a lucid comparative setting for our proposed multistage approach and nonuniform fractionation scheme. Such a comparison will enable us to demonstrate the advantages of the proposed methods for potential consideration in practice. For this reason, before we introduce

our proposed models in the next section, we present the underlying basic model of the static approach that ignores the uncertain evolution of the tumor and OAR over future fractions.

We refer to this model as the static model and denoted by (**S**) below. The model determines an optimal FM that minimizes the fraction-specific squared deviation penalty subject to the requirements of a uniform fractionation scheme. It is formulated as

$$\begin{aligned} &\min \ f_1(\mathbf{x}_1, \ell_1) \\ &\text{subject to } (\mathbf{x}_1, \mathbf{y}_1, \mathbf{z}_1, \ell_1) \in \mathcal{S}_1(\xi_1) \cap \mathcal{U}_1^0, \end{aligned} \tag{S}$$

and implemented in a static fashion. Let $(\mathbf{x}_1^\star, \mathbf{y}_1^\star)$ denote the optimal FM obtained by solving the static model (**S**). Under the static approach, the same FM $(\mathbf{x}_1^\star, \mathbf{y}_1^\star)$ is used in every fraction going forward (i.e., for fractions $n = 2, \ldots, N$). Since the optimization model only uses information available at the beginning of the treatment and does not consider any future prediction, (**S**) can be classified as a single-stage model (in contrast to the multistage models proposed in this paper). As mentioned in [23], this model is representative of and analogous with what is utilized in practice.

As expected, the optimal FM $(\mathbf{x}_1^\star, \mathbf{y}_1^\star)$ computed based on the static model (**S**) is likely to be suboptimal for future fractions $n = 2, \ldots, N$ when the tumor and OAR may have evolved. Such suboptimality may result in undesirable ramifications, as will be illustrated in our computational experiments. Also, the fractionation scheme lends itself to obtaining new CT scans during a course of treatment (e.g., adaptive radiation therapy, [24]). When the fractionation scheme is implemented under a static approach, however, it does not take advantage of a planning that considers future potential anatomical changes at the initial planning stage. The multistage models that we describe next are intended to address these shortcomings of the static approach in a fractionated setting.

3 Deterministic Multistage Formulations

A deterministic multistage setting is suitable when the patient's current condition is known (from the latest CT scan) and a prediction for each subsequent fraction (one prediction for

each future fraction) is available from the beginning of the treatment. Such future predictions are also known as the *lookahead information*. The predictions are available in the form of a sequence of predicted CT scans $\{\xi_n\}_{n=2}^N$ (note that ξ_1 is already known from the initial CT scan). We highlight the distinction between having a single-point prediction for each future fraction (deterministic) rather than multiple predictions in the form of scenarios with different probabilities at each fraction (stochastic).

Using the CT-scan information, the dose-deposition matrices $\mathbf{A}_n(\xi_n)$ are computed for $n = 1, \ldots, N$. Since the deterministic multistage models accommodate structural evolution through CT-scan information $\{\xi_n\}_{n=1}^N$, they are able to provide FMs that are tailored to this information. From a clinical perspective, this is a hypothetical setting (unless, predictive methods are used proactively); yet, the setting provides a foundation for academic research which incorporates future predictions (perfect or otherwise) and sets the stage for a more general stochastic setting that accommodates multiple predicted scenarios.

3.1 Uniform Deterministic Multistage Model

The static model (**S**) discussed in the previous section relies on the most basic implementation of the uniform fractionation scheme by completely ignoring evolution of the tumor and OAR over future fractions. This fractionation scheme may also be implemented in the context of the deterministic multistage setting of interest here leading to the following model which is referred as the uniform deterministic multistage model and denoted by (**UD**):

$$\begin{aligned} \min \ & \sum_{n=1}^{N} f_n(\mathbf{x}_n, \ell_n) \qquad (\mathbf{UD}) \\ \text{subject to } & (\mathbf{DP});\ (\mathbf{x}_n, \mathbf{y}_n, \mathbf{z}_n, \ell_n) \in \mathcal{S}_n(\xi_n) \cap \mathcal{U}_n^0, \quad \forall n = 1, \ldots, N. \end{aligned}$$

In addition to constraints (**DP**), the fraction-specific dose prescription decisions satisfy $(\ell_n, \mathbf{z}_n) \in \mathcal{U}_n^0$. The latter enforces the requirements for the uniform fractionation scheme. The fraction-specific decisions must additionally belong to the set $\mathcal{S}_n(\xi_n)$. The model aims to minimize the SDP computed across all N fractions.

It is worthwhile to note that, due to the uniform fractionation scheme, the fraction-specific dose prescriptions of the uniform deterministic multistage model (**UD**) must be trivially set to

$\ell_n = \frac{L^{\text{tumor}}}{N}$ and $z_n^{(i)} = \frac{u^{(i)}}{N}$, the constraints (**DP**) are rendered redundant, and the formulation decomposes by fractions reducing the model to

$$\sum_{n=1}^{N} \Big(\min \ \big\{ f_n\big(\mathbf{x}_n, \ell_n\big) \ \big| \ (\mathbf{x}_n, \mathbf{y}_n, \mathbf{z}_n, \ell_n) \in \mathcal{S}_n(\xi_n) \cap \mathcal{U}_n^0 \big\} \Big). \tag{7}$$

The above observation implies that there is no value in incorporating the lookahead information in RTP under uniform fractionation scheme. In other words, the uniform fractionation scheme does not lend the optimization model enough freedom to take advantage of the lookahead knowledge. Hence, there is a strong motivation to explore less restrictive multistage models capable of effectively utilizing predicted tumor evolution information in the fractionated setting. This leads us to the nonuniform multistage models that we discuss next.

3.2 Nonuniform Deterministic Multistage Model

To model the nonuniform fractionation scheme, we relax the restrictions on the fraction-specific dose prescriptions. We achieve this by introducing $\epsilon > 0$ which expands the set of feasible fraction-specific dose prescriptions $\mathcal{U}_n^\epsilon$. Moreover, in relation to the feasible sets used in (**UD**), the sets of feasible fraction-specific dose prescriptions now satisfy $\mathcal{U}_n^\epsilon \supset \mathcal{U}_n^0$ for $n = 1, \ldots, N$. The resulting optimization model under nonuniform fractionation is then given by

$$\begin{aligned} \min \ & \sum_{n=1}^{N} f_n(\mathbf{x}_n, \ell_n) \\ \text{subject to } & (\mathbf{DP}); \ (\mathbf{x}_n, \mathbf{y}_n, \mathbf{z}_n, \ell_n) \in \mathcal{S}_n(\xi_n) \cap \mathcal{U}_n^\epsilon, \quad \forall n = 1, \ldots, N. \end{aligned} \tag{ND}$$

Notice that in the above model, the dose-prescription decision variables ($\mathbf{z}_n$, ℓ_n) are no longer trivially determined for every fraction. Therefore, the fraction-specific dose prescriptions ($\mathbf{z}_n$, ℓ_n) as well as the FMs ($\mathbf{x}_n, \mathbf{y}_n$) are adaptive in response to the future lookahead information.

A couple of observations regarding (**ND**) are in order. Firstly, as a consequence of $\mathcal{U}^\epsilon \supset \mathcal{U}_n^0$, for any fraction n, we have $\{\mathcal{S}_n(\xi_n) \cap \mathcal{U}_n^\epsilon\} \supseteq \{\mathcal{S}_n(\xi_n) \cap \mathcal{U}_n^0\}$. Therefore, it is evident that the optimal objective function value of the nonuniform deterministic multistage model (**ND**) is at most the optimal objective function value of (**UD**). Secondly, it is worthwhile to mention that ($\mathbf{z}_n$, ℓ_n) are coupled across fractions through constraints (**DP**). Therefore, unlike (**UD**), the formulation of (**ND**) does not decompose by fractions.

Observe that neither of the deterministic multistage models ((**UD**) and (**ND**)) take total dose (Overall or OAR) into consideration explicitly. From a practical point of view, a precise delivery plan is desirable. However, if this precise delivery comes at the cost of relatively higher TD-Overall and TD-OAR, implying greater exposure for the patient, then such a plan is not ideal. To address this issue, we revise the nonuniform deterministic multistage model (**ND**) as

$$\begin{aligned} \min \ & \sum_{n=1}^{N} f_n(\mathbf{x}_n, \ell_n) && \text{(RND)} \\ \text{subject to } & (\mathbf{x}_n, \mathbf{y}_n, \mathbf{z}_n, \ell_n) \in \mathcal{S}_n(\xi_n) \cap \mathcal{U}_n^{\epsilon}, \quad \forall n = 1, \ldots, N, \\ & \sum_{n=1}^{N} \sum_{i \in \mathcal{T}} \sum_{v \in \mathcal{V}_n^{(i)}} x_{vn} \leq \bar{\tau}. && (8) \end{aligned}$$

The additional constraint (8) in the model bounds the feasible AD quantity by a given upper bound $\bar{\tau} \in \mathbb{R}_+$. Specifically, if we set $\bar{\tau} = \sum_{n=1}^{N} \sum_{i \in \mathcal{T}} \sum_{v \in \mathcal{V}_n^{(i)}} x_{vn}^{\star UD}$, then the AD prescribed by (**RND**) is bounded above by the optimal AD under (**UD**).

It is not guaranteed that the (**UD**) results in a lower total dose when compared to (**ND**). But when it does, then the second constraint in the revised model is active. However, since the revised model uses the optimal solution (**UD**), the additional constraint results in added computational expense resulting from solving two optimization problems. Procedure 1 summarizes how to make use of the proposed multistage models presented so far.

Procedure 1 Nonuniform Deterministic Fractionation Procedure.

1: **Input:** Number of fractions, N; total dose prescription $\mathbf{u}$ and L^{tumor}; current CT-scan information ξ_1 and a prediction of structural evolution $\{\xi_n\}_{n=2}^{N}$.

2: Compute the dose-deposition matrices $\mathbf{A}_n$ for $n = 1, \ldots, N$.

3: Solve the uniform deterministic model (**UD**) and obtain the optimal solution $\mathbf{x}_n^{\star UD}$ for $n = 1, \ldots, N$. Using the optimal solution, compute AD for (**UD**).

4: Using AD from (**UD**) as $\bar{\tau}$, instantiate and solve the revised nonuniform model (**RND**). Obtain the optimal solution $(\mathbf{x}_1^{\star}, \mathbf{y}_1^{\star}, \mathbf{z}_1^{\star}, \ell_1^{\star})$.

5: **Output:** The optimal dose prescriptions $(\mathbf{z}_1^{\star}, \ell_1^{\star})$ and the beamlet intensities $\mathbf{y}_1^{\star}$.

3.3 Numerical Results for a Comparison of the Deterministic Models

We now turn our attention to the numerical evaluation of the deterministic multistage models presented so far, viz., (**S**), (**UD**), (**ND**), and (**RND**). Our first objective is to establish the relative performance for each of the four models in terms of SDP, TD-Overall, TD-OAR, and TUD, as defined in Section 2.2. Our second objective is to demonstrate the superiority of the (**RND**) with respect to all metrics of interest. To this end, we utilize the prostate cancer CT scans provided by [25]. To the best of our knowledge, this is the only dataset available online (http://faculty.washington .edu/archis/spintfracdata.zip). The dataset provides five prostate CT scans. For the numerical experiments regarding our deterministic multistage models, we choose three of the provided scans that reasonably represent a prostate cancer patient's structural evolution over $N = 3$ fractions. We then preprocess[1] all dose-deposition matrices to suit our experimental setting and objectives. These three scans (labeled as Scan 1, Scan 3, and Scan 4 in our data files), in turn, are used to generate six ($3! = 6$) scan sequences illustrated in Table 1.

Scan Sequences	First-Stage	Second-Stage	Third-Stage
1	Scan 1	Scan 4	Scan 3
2	Scan 1	Scan 3	Scan 4
3	Scan 3	Scan 1	Scan 4
4	Scan 3	Scan 4	Scan 1
5	Scan 4	Scan 1	Scan 3
6	Scan 4	Scan 3	Scan 1

Table 1: Scan Sequences Used to Generate Numerical Instances for Deterministic Models.

We assume that the differences between the scans represent a patient's physical structures evolving between fractions. We use two sets of parameters denoted by $P1$ and $P2$ that are summarized in Table 2 and differ in the values for weights (w_n^+, w_n^-). The parameter set $P1$ penalizes tumor underdose and overdose equally (i.e., $w_n^+ = w_n^- \ \forall n$) whereas $P2$ heavily penalizes under dosage of the tumor (i.e., $w_n^+ \ll w_n^- \ \forall n$). When combined with the scan sequences summarized in Table 1, parameter sets $P1$ and $P2$ result in a total of twelve instances, (i.e., six instances each for $P1$ and $P2$, respectively) of the deterministic multistage models.

[1]For the purposes of numerical results presented in this paper, all dose-deposition matrix instances were obtained from [25] and were generated by the authors' in-house phantom creator software PhanC written in MATLAB [26].

Set	N	L^{tumor}	u^{rectum}	u^{bladder}	$u^{\text{left femur}}$	$u^{\text{right femur}}$	w^+	w^-
$P1$	3	81	75	79	55	55	0.5	0.5
$P2$	3	81	75	79	55	55	0.001	0.999

Table 2: Parameter Sets $P1$ and $P2$.

3.3.1 Impact of Nonuniform Fractionation on the Metrics of Interest and DVHs

For the first set of experiments, we consider the most general (relaxed) versions of the nonuniform deterministic multistage models obtained by using $\epsilon = M$ in the description of the set $\mathcal{U}_n^\epsilon$ (see (**DP**)). In Table 3, we report the resulting average values of metrics SDP, TD-Overall, TD-OAR, and TUD, computed over all numerical instances under $P1$ (six scan sequences) and $P2$ (six scan sequences), for each model. Also, although TUD is computed for each fraction individually, the average performance over the $N = 3$ fractions is reported.

	Parameter Set $P1$				Parameter Set $P2$			
	SDP	TD-Overall	TD-OAR	TUD	SDP	TD-Overall	TD-OAR	TUD
(**S**)	184420.0128	4.2247	8.8811	50.5555	283651.5815	4.0502	8.0958	36.5689
(**UD**)	358.6021	4.2375	8.2729	48.7630	196.0174	4.0727	6.7470	3.1840
(**ND**)	220.2699	4.6349	8.6301	48.3648	3.9990	4.2457	7.6717	9.0562
(**RND**)	222.3800	4.2375	7.9658	48.4390	6.6025	4.0715	6.1853	1.2108

Table 3: A Comparison of Metrics of Interest for Deterministic Models under Parameter Sets $P1$ and $P2$: Comprehensive Numerical Results Reporting Average Values over All Numerical Instances.

The results indicate the severe inadequacy of the static approach across both parameter sets, in terms of SDP, TD-OAR, and TUD. This observation validates our idea that simply using the same FM for all fractions in a setting where patient structural evolution is present may lead to undesirable outcomes (increased exposure to OAR and reduced radiation precision). The multistage models that utilize the prediction information to adapt FMs across fractions address the shortcoming of the static approach. The improvement is most evident in the SDP results under both settings. The value of nonuniform fractionation is evident by comparing the SDP results of (**UD**) and (**ND**). Since both the models aim to minimize the SDP and (**UD**) imposes additional restrictions on how the overall prescription is distributed into fraction-specific prescriptions, the SDP is higher (62.8%) for (**UD**) when compared to (**ND**). Notice that the

value of nonuniform fractionation is even higher under ($P2$).

The nonuniform deterministic multistage model (**ND**) is the most relaxed variant among the deterministic models. This is reflected in the fact that SDP is lowest for (**ND**) under both the settings. However, the TD (overall and OAR) for (**ND**) is higher compared to other models. The revised model (**RND**) addresses this issue and obtains solutions that are not only precise but also require lower overall radiation exposure. In this regard, (**RND**) demonstrates the desired *win-win* outcome and constitutes a collectively superior approach. Finally, when the weights are chosen to incentivize avoiding tumor underdosing ($P2$), TUD reduces for all the models studied (compare the TUD columns under the two settings). It is also worthwhile to note that under ($P2$) the exposure of OAR to radiation (radiation toxicity) is also reduced while improving precision (lower SDP). This last observation indicates the importance of considering an objective that emphasizes tumor underdosing as opposed to a symmetric precision-based objective.

As we have mentioned earlier, a popular method for comparing radiation plans is through DVHs [1, 22]. These illustrations capture the proportion of a particular patient structure which receives more than a specified amount of dosage. Out of the twelve instances, we present DVHs across the two parameter settings ($P1$ and $P2$) for Scan Sequence 1. From the two collections of DVH Figures 1 and 2, we determine that for this scan sequence, the static model is "fortunate" and provides comparable results for the femur structures (1(c),1(d), 2(c),2(d)). On the other hand, the DVHs show the static model is exposing the patient's bladder to infeasible amounts of radiation (1(b), 2(b)). This observation accompanied with the numerical results summarized above indicate the need to reevaluate the use of static approach for RTP. In regards to the other three multistage models, the illustrations are much more analogous across the varying structures, weights, and performance metrics. Overall, the visual comparison is in accordance with the results from the numerical output.

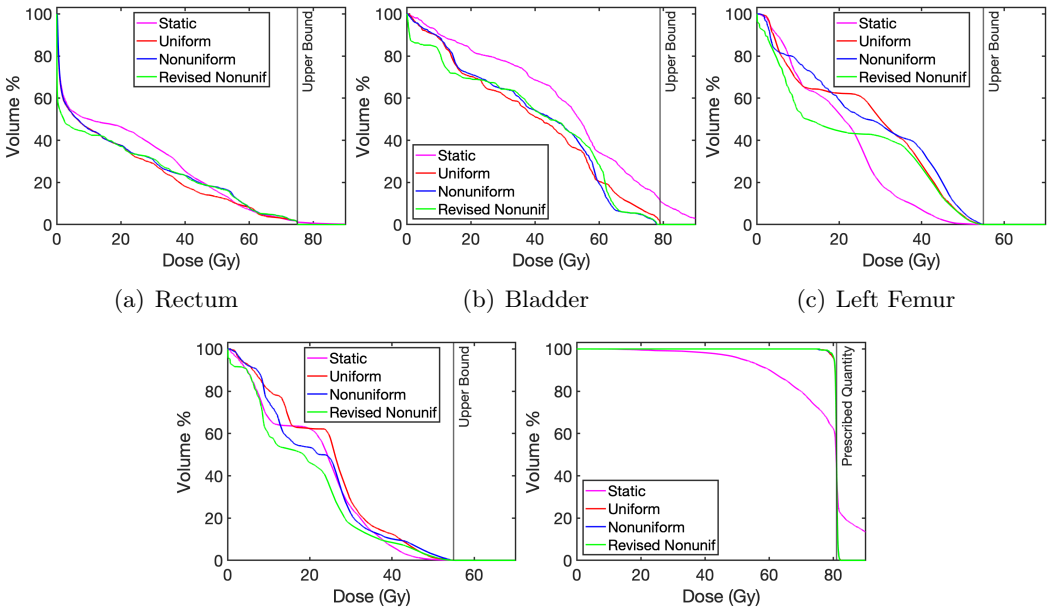

(a) Rectum (b) Bladder (c) Left Femur

(d) Right Femur (e) Tumor

Figure 1: An Illustrative Comparison of OAR and Prostate Tumor DVHs for Deterministic Models under Scan Sequence 1 (Scans 1,4,3) and Parameter Set $P1$.

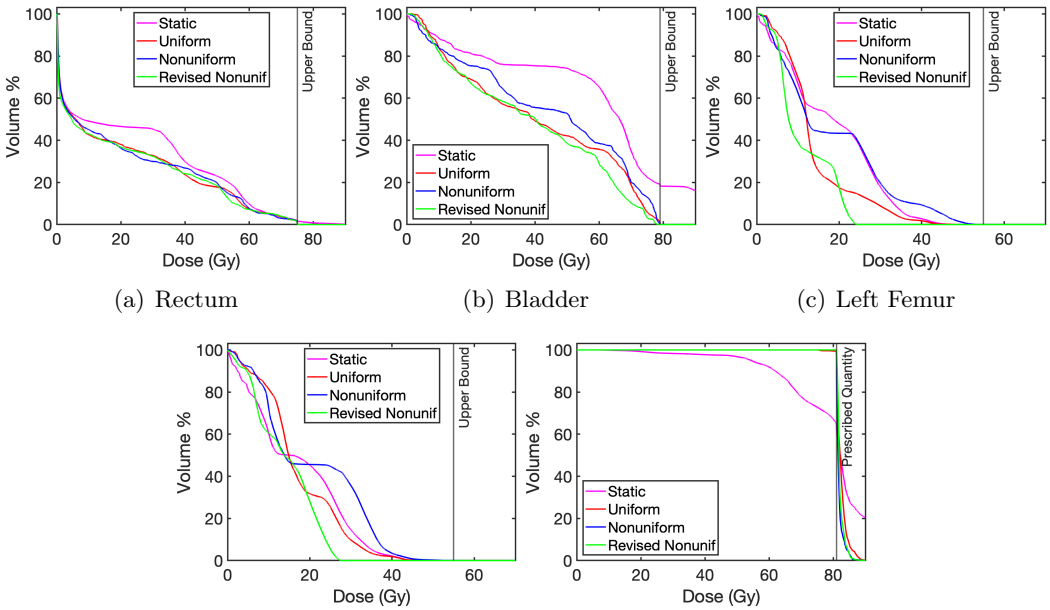

(a) Rectum (b) Bladder (c) Left Femur

(d) Right Femur (e) Tumor

Figure 2: An Illustrative Comparison of OAR and Prostate Tumor DVHs for Deterministic Models under Scan Sequence 1 (Scans 1,4,3) and Parameter Set $P2$.

3.3.2 Impact of the Degree of Nonuniformity

While the nonuniform fractionation models (**ND**) and (**RND**) provide flexibility in choosing the fraction-specific dose prescriptions, the resulting values for ℓ_n and $\mathbf{z}_n$ may deviate significantly between fractions. For example, (**RND**) assigns a tumor dose schedule of

$\ell_n = (10.39, 30.00, 40.61)$ for $n = 1, 2, 3$ in one case of our numerical experiment. Such drastic variation between fractions is clinically undesirable, and, hence, in the next set of experiments, we explore the impact of varying the degree of nonuniformity in fractionation.

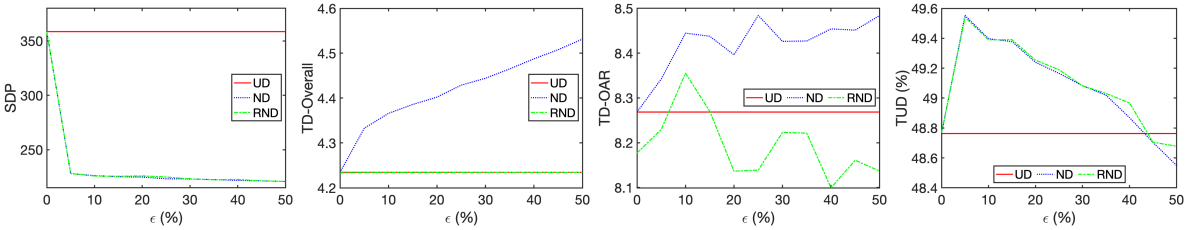

(a) SDP (b) TD-Overall (c) TD-OAR (d) TUD

Figure 3: An Evaluation of Deterministic Models' Performance across Metrics of Interest for Varying Degrees of Nonuniformity ($\epsilon \in [0, 0.50]$) under Parameter Set $P1$.

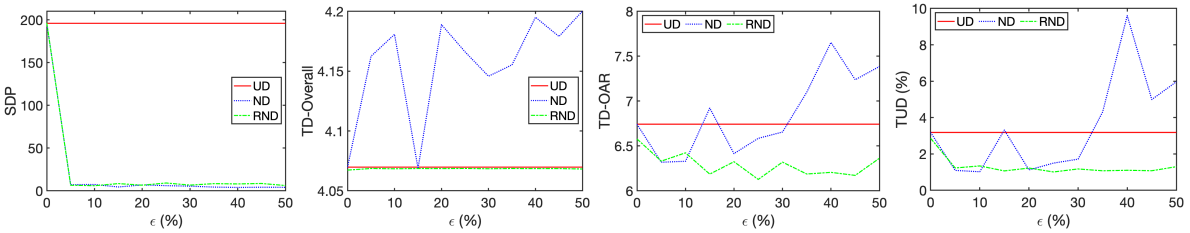

(a) SDP (b) TD-Overall (c) TD-OAR (d) TUD

Figure 4: An Evaluation of Deterministic Models' Performance across Metrics of Interest for Varying Degrees of Nonuniformity ($\epsilon \in [0, 0.50]$) under Parameter Set $P2$.

Recall that the degree of nonuniformity is determined by the value of $\epsilon \in [0, M]$ used in the description of the set $\mathcal{U}_n^\epsilon$ for any n. While $\epsilon = M$ results in the highest degree of nonuniformity, a value of $\epsilon = 0$ implies a uniform fractionation scheme. We keep all the other parameters in $P1$ and $P2$ the same while varying ϵ between 0.05 to 0.50. This implies that if we were to restrict (**ND**) or (**RND**) to, say 10% nonuniformity, the fraction-specific tumor prescriptions for each fraction must be within $[24.3, 29.7]$.

Figures 3 and 4 present the overall trend of SDP, TD-Overall, TD-OAR, and TUD for (**UD**), (**ND**), and (**RND**) as we vary the degree of nonuniformity. The (**RND**) outperforms the other models in terms of SDP. Moreover, there is only a limited variation in SDP when the value of ϵ is increased. It is worthwhile to note that even when only 5% of deviation is allowed, we observe significant improvement in SDP under both the parameter settings. The results also indicate that the performance of (**RND**) is comparable to that of (**ND**), measured in terms of SDP. On

the other hand, the revised model outperforms other models in terms of TD-OAR and TUD.

The deterministic multistage models utilize a perfect prediction of future evolution. However, one should expect the presence of errors in such predictions. Motivated by the performance of the multistage models in deterministic settings, we next present stochastic multistage models. These stochastic models utilize a certain representation of the future evolution that accounts for prediction errors. This extension brings forth a practical approach that requires the departure from a deterministic optimization toward stochastic optimization methods.

4 Stochastic Multistage Formulations

In addition to uncertainties associated with future status prediction, there are two possible sources of stochasticity encountered during radiation therapy [16, 17, 27, 28, 29]. The first source pertains to treatment geometry that includes errors in setting up the patient on the treatment device and errors resulting from breathing and peristaltic movements. We refer to such sources of stochasticity as intrafractional uncertainty. The second source is the interfractional uncertainty which includes the evolution of structures throughout the treatment. Previous work on optimization-based RTP models that explicitly accommodate stochasticity can be classified as robust optimization models (e.g., [30, 31, 32]), risk-based optimization models [33, 34, 35], or risk-neutral stochastic programming models [17, 36]. The models we present in this section have potential to accommodate interfractional uncertainty in the form of a patient's structural volume evolution as well as uncertainties associated with future predictions. Similar to Section 3, we begin by first presenting the uniform stochastic multistage formulation. Afterward, we present the revised nonuniform stochastic formulation. In the stochastic models, we aim to minimize the expected value of SDP computed across all N fractions.

In the stochastic multistage setting, as in the case of the deterministic setting, we know the patient's current condition from the latest CT scan. However, unlike the deterministic setting where only a single prediction of structure evolution is utilized, the stochastic models explicitly account for errors in predictions. With numerical computations in mind, we depict the possible sequence of patient states in a form of a scenario tree [37] (see Figure 5) as explained next.

A scenario tree can be viewed as a discretization of the underlying stochastic process $\{\tilde{\xi}\}$ associated with the patient's structural evolution using a set of nodes $\mathcal{J}$. The tree is arranged in stages corresponding to each fraction. The first node of the tree, also known as the root node, corresponds to the current state (ξ_1) and nodes in subsequent stages ($n = 2, \ldots, N$) represent possible alternative states in the corresponding fraction. For example, $\xi_3^1, \xi_3^2, \xi_3^3$, and ξ_3^4 represent four alternative states during Fraction 3 as shown in Figure 5. The scenario tree captures the precedence relationships (dependencies) between states in one fraction to those in the next fraction. The scenario tree also encodes $p_n^{(j)}$ as the probability of encountering node $j \in \mathcal{J}$ in fraction $n = 1, \ldots, N$.

The sequence of nodes, starting from the root node to a leaf node, is referred to as a *scenario* or a sample path. A scenario, therefore, represents a possible path of structural evolution starting from the current state of the patient. We denote the set of all possible scenarios by the set $\mathcal{K}$ and use the notation $j \in [k]$ to denote that the node $j \in \mathcal{J}$ belongs to scenario $k \in \mathcal{K}$. Notice that the number of scenarios represented on a tree is equal to the number of leaf nodes.

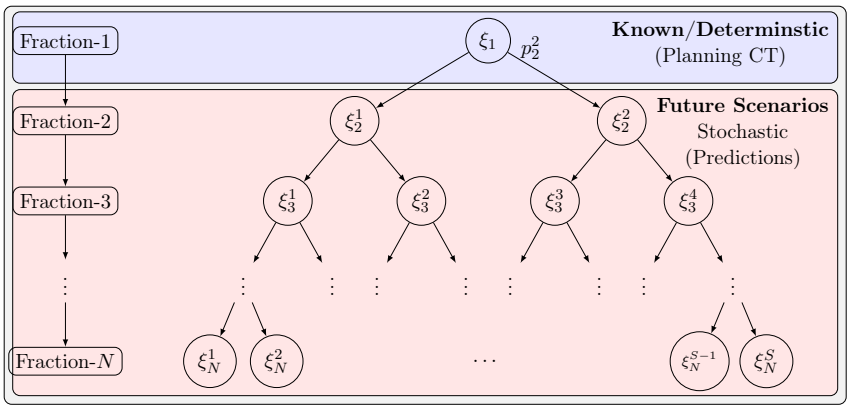

Figure 5: A Generic Scenario Tree Representation

4.1 Uniform Stochastic Multistage Model

The uniform stochastic multistage model (the analog of (**UD**)) is presented in the following nested form:

$$\min \; f_1(\mathbf{x}_1, \ell_1) + \mathbb{E}_{|\xi_{[1]}}\Big[\min f_2(\mathbf{x}_2, \ell_2) + \cdots + \mathbb{E}_{|\xi_{[N-1]}}\Big[\min f_N(\mathbf{x}_N, \ell_N)\Big]\Big] \qquad (\mathbf{US})$$

$$\text{subject to } (\mathbf{x}_n, \mathbf{y}_n, \mathbf{z}_n, \ell_n) \in \mathcal{S}_n(\tilde{\xi}_n) \cap \mathcal{U}_n^0, \quad \forall n = 1, \ldots, N, \; a.s.$$

In the nested form, the expectations are taken with respect to future uncertainty conditional on information that is already realized, i.e., $\xi_{[n]} := \{\xi_i \mid i = 1, \ldots, n\}$.

When a scenario tree representation is used, the expectations can be replaced by summation over all the nodes in a given stage of the scenario tree. By duplicating the decision variables for each node, the stochastic program can be stated as a single large optimization problem known as the extensive scenario form. We refer the reader to stochastic programming textbooks [38, 37] for more details on how to construct such extensive scenario forms. Consequently, the optimal solution of a stochastic multistage model will provide FMs for all the nodes in a scenario tree. The FM corresponding to the root node $(\mathbf{x}_1^\star, \mathbf{y}_1^\star)$ is recommended for treating in the first fraction. The FMs $(\mathbf{x}_n^{j,\star}, \mathbf{y}_n^{j,\star})$ for the nodes $j \in \mathcal{J}$ in future stages $(n = 2, \ldots, N)$ are advisory in nature, with a possibility of updating them in the future.

As is the case in deterministic uniform fractionation, the stochastic uniform fractionation model in (**US**) also decomposes into smaller optimization problems. In the case of (**US**), this decomposition is by nodes in the scenario tree. This feature is captured in the following result.

Proposition 4.1. *Under a uniform fractionation scheme,* (**US**) *decomposes into a collection of individual FM optimization problems corresponding to nodes $j \in \mathcal{J}$ in the scenario tree. That is,* (**US**) *is equivalent to*

$$\sum_{j \in \mathcal{J}} p_n^j \min \left\{ f_n(\mathbf{x}_n, \ell_n) \;\middle|\; (\mathbf{x}_n, \mathbf{y}_n, \mathbf{z}_n, \ell_n) \in \mathcal{S}_n(\xi_n^j) \cap \mathcal{U}_n^0 \right\}.$$

Proof. Since $(\mathbf{z}_n, \ell_n) \in \mathcal{U}_n^0$, we have that fraction-specific dose prescriptions satisfy $\ell_n = \frac{L^{\text{tumor}}}{N}$ and $z_n^{(i)} = \frac{u^{(i)}}{N}$ for all $i \in \mathcal{O}$ (see (2)). Consequently, we can project the set $\mathcal{S}_n(\xi_n^j)$ to a linear subspace where the FM decisions $(\mathbf{x}_n, \mathbf{y}_n)$ satisfy (3) and (4). Since constraints (3) and (**DP**.b) are specific to a realization in a fraction (for $z_n^{(i)} = \frac{u^{(i)}}{N}$ $\forall i \in \mathcal{O}$), the optimization problem decomposes by nodes in the scenario tree. Therefore, the expectation-valued objective function can be written as the sum of node-specific objective function that are weighted by the probability of encountering the node. □

The above result illustrates that the value of lookahead information (either stochastic or deterministic) is zero when uniform fractionation scheme is adopted. Therefore, if the clini-

cal practice forbids the adoption of nonuniform fractionation, then solving a fraction-specific optimization problem that only uses current CT scan information (ξ_1) will suffice.

4.2 Nonuniform Stochastic Multistage Model

Similar to the deterministic setting, we relax the fractionation scheme and allow the optimization model to determine fraction-specific dose prescriptions. However, a nonuniform model may provide a precise approach that results in an ideal SDP but drastically higher TD (Overall and OAR), as was observed in the numerical experiments with deterministic models (see Section 3.3). Given that we strive to obtain *win-win* outcomes when comparing TD (Overall and OAR) and SDP, the AD quantities obtained from solving (**US**) are utilized to bound the corresponding quantities in the nonuniform model. Unlike the deterministic setting where we have a single prediction, in the stochastic setting, we have multiple scenarios. To develop a suitable bound, we define the realized AD along a scenario $k \in \mathcal{K}$ as

$$\tau(k) = \sum_{n=1}^{N} \sum_{i \in \mathcal{T}} \sum_{v \in \mathcal{V}_n^{(i)}} \sum_{j \in \mathcal{J}} \mathbb{1}_{j \in [k]} x_{vn}^j, \tag{9}$$

where $\mathbb{1}_{(\bullet)}$ is an indicator function. When an optimal solution is used to compute the realized AD, we will denote it by $\tau^\star(k)$. Using the above, we state the nonuniform stochastic multistage problem as

$$\min \;\; f_1(\mathbf{x}_1, \ell_1) + \mathbb{E}_{|\xi_{[1]}} \Big[\min f_2(\mathbf{x}_2, \ell_2) + \cdots + \mathbb{E}_{|\xi_{[N-1]}} \Big[\min f_N(\mathbf{x}_N, \ell_N) \Big] \Big] \qquad (\mathbf{RNS})$$

$$\text{subject to } (\mathbf{x}_n, \mathbf{y}_n, \mathbf{z}_n, \ell_n) \in \mathcal{S}_n(\tilde{\xi}_n) \cap \mathcal{U}_n^\epsilon, \qquad \forall n = 1, \ldots, N, \; a.s.,$$

$$\sum_{n=1}^{N} \sum_{i \in \mathcal{T}} \sum_{v \in \mathcal{V}_n^{(i)}} x_{vn} \leq \tau(k) \qquad \forall k \in \mathcal{K}.$$

The above model determines the fraction-specific dose prescriptions and FMs that are hedged against the possible errors in predicting the evolution of the structures in the future. The second constraint ensures that the AD prescribed by (**RNS**) is within an upper bound given by $\tau(k)$ for each scenario $k \in \mathcal{K}$. Similar to (**RND**), we use upper bounds computed from the optimal solution of (**US**).

In the presence of prediction errors, we adopt Procedure 2 under a nonuniform fractionation scheme. Following Proposition 4.1, in Step 3, we can solve the uniform node-specific FM opti-

Procedure 2 Nonuniform Stochastic Fractionation

1: **Input:** Number of fractions, N; dose prescription specifying $\mathbf{u}$ and L^{tumor}; current CT-scan information ξ_1; a scenario tree representing possible scenarios of structural evolution $\{\xi_n^j\}_{n=2}^N$ and $j \in \mathcal{J}$.

2: Compute the dose-deposition matrices $\mathbf{A}_n^i$ for all nodes on a scenario tree ($n = 1, \ldots, N$, $j \in \mathcal{J}$).

3: Solve the uniform stochastic model (**US**) and obtain the optimal solution $\mathbf{x}_n^{\star US}$ for $n = 1, \ldots, N$ and $j \in \mathcal{J}$.

4: Compute the AD $\tau(k)$ for all $k \in \mathcal{K}$.

5: Instantiate and solve the revised nonuniform model (**RNS**). Obtain the optimal solution.

6: **Output:** The optimal dose prescriptions $(\mathbf{z}_1^\star, \ell_1^\star)$ and the beamlet intensities $\mathbf{y}_1^\star$.

mization problem for each node of the scenario tree. We next turn to numerical experimentation in order to draw comparison between (**US**) and (**RNS**).

4.3 Numerical Results Comparing Stochastic Models

Again using the CT scan data provided by [26], we conduct numerical experiments with the stochastic multistage models to achieve the following two objectives. First, we quantify the value of nonuniform fractionation in a stochastic problem setting. Second, we establish the value of a stochastic solution when compared to the potential approaches that ignore uncertainty entirely.

For the case where $N = 3$, we consider the scan sequences summarized in Table 4 resulting in four distinct scenario trees labeled ST1, ST2, ST3, and ST4. We set the conditional probabilities at all non-terminal nodes to 0.5. Generating the collection of scenario trees requires assigning a variety of combinations of nodes at each stage. Table 4 outlines the composition of each of the

Scenario Tree	First-Stage Node	Second-Stage Nodes	Third-Stage Nodes
ST1	Scan 2	Scans 1,4	Scans 5,3
ST2	Scan 1	Scans 2,5	Scans 3,4
ST3	Scan 4	Scans 2,3	Scans 1,5
ST4	Scan 5	Scans 1,3	Scans 2,4

Table 4: Scan Sequences Used to Generate Scenario Trees for Stochastic Multistage Models.

four scenario trees considered. All scenario trees have a fixed first-stage scan, two second-stage nodes (predictions), and two third-stage nodes (predictions) which provide four unique scenarios per tree. Instances of the stochastic multistage models (**US**) and (**RNS**) are generated and solved for ST1, ST2, ST3, and ST4. We report the comprehensive results for all the metrics described in Section 2.2.

4.3.1 A Comparison of the Metrics of Interest under Stochastic Models

Table 5 summarizes the comprehensive numerical results of stochastic multistage models (**US**) and (**RNS**). We report the average, standard deviation (std. dev.), and range of the metrics of interest computed across all numerical instances, i.e, for all of the scenario trees (ST1, ST2, ST3, and ST4) under $P1$ and $P2$. For (**RNS**), we also present the percentage improvement in the average values of metrics relative to the results obtained from (**US**) computed.

Parameter Set $P1$					
		SDP	TD-Overall	TD-OAR	TUD
(**US**)	Average	372.4063	4.0439	8.4727	47.8338
	Std. dev.	29.0147	0.1546	0.2489	0.1153
	Range	[347.7997 , 411.0633]	[3.8792 , 4.2293]	[8.3057 , 8.8420]	[47.7138 , 47.9886]
(**RNS**)	Average	331.6761	4.0409	8.1663	47.6843
	Std. dev.	12.0001	0.1550	0.5814	0.3375
	Range	[313.8627 , 339.6415]	[3.8776 , 4.2280]	[7.6308 , 8.9219]	[47.2869 , 48.0817]
	Improve (%)	10.9370	0.0742	3.6163	0.3125
Parameter Set $P2$					
		SDP	TD-Overall	TD-OAR	TUD
(**US**)	Average	157.3246	3.8332	7.2790	3.8876
	Std. dev.	44.9074	0.1451	0.1982	0.3612
	Range	[127.0373 , 222.1330]	[3.6510 , 4.0008]	[7.0889 , 7.5428]	[3.6562 , 4.4180]
(**RNS**)	Average	23.2651	3.8305	6.3381	1.4558
	Std. dev.	3.1202	0.1455	0.2426	0.5875
	Range	[18.6973 , 25.7280]	[3.6483 , 4.9991]	[6.1182 , 6.5973]	[0.9338 , 2.1868]
	Improve (%)	85.2120	0.0704	12.9262	62.8100

Table 5: A Comparison of Metrics of Interest for Stochastic Multistage Models under Parameter Sets $P1$ and $P2$: Comprehensive Numerical Results Reporting Average Values, Standard Deviations, and Ranges over All Numerical Instances.

A closer examination of the results in Table 5 reveals the clear advantages of choosing the stochastic multistage model with a nonuniform fractionation scheme. Across both parameter sets, the improvement in regards to TD-Overall is minimal. However, (**RNS**) provides improvements in SDP, TD-OAR, and TUD. The advantages of stochastic nonuniform fractionation models is more pronounced when we consider $P2$, notice 85.21% and 62.81% improvements in SDP and TUD, respectively.

To further illustrate the comparison between (**US**) and (**RNS**), we present the box-and-whisker plots in Figures 6 generated using results from Table 5. In a box-and-whisker plot, the top and bottom of the box represents the 75^{th} and 25^{th} quantiles, respectively, whereas the central red line indicates the median and the whiskers are the extreme values. The results reveal the significant improvement in terms of SDP in (**RNS**) for both parameter sets $P1$ and $P2$. Notice that the minimum SDP obtained from (**US**) is higher than the maximum SDP obtained from (**RNS**), indicating that the nonuniform fractionation scheme dominates the uniform fractionation scheme across all the representations of uncertainty considered in our experiment. The dominance is much more significant for $P2$ when compared to $P1$. The two

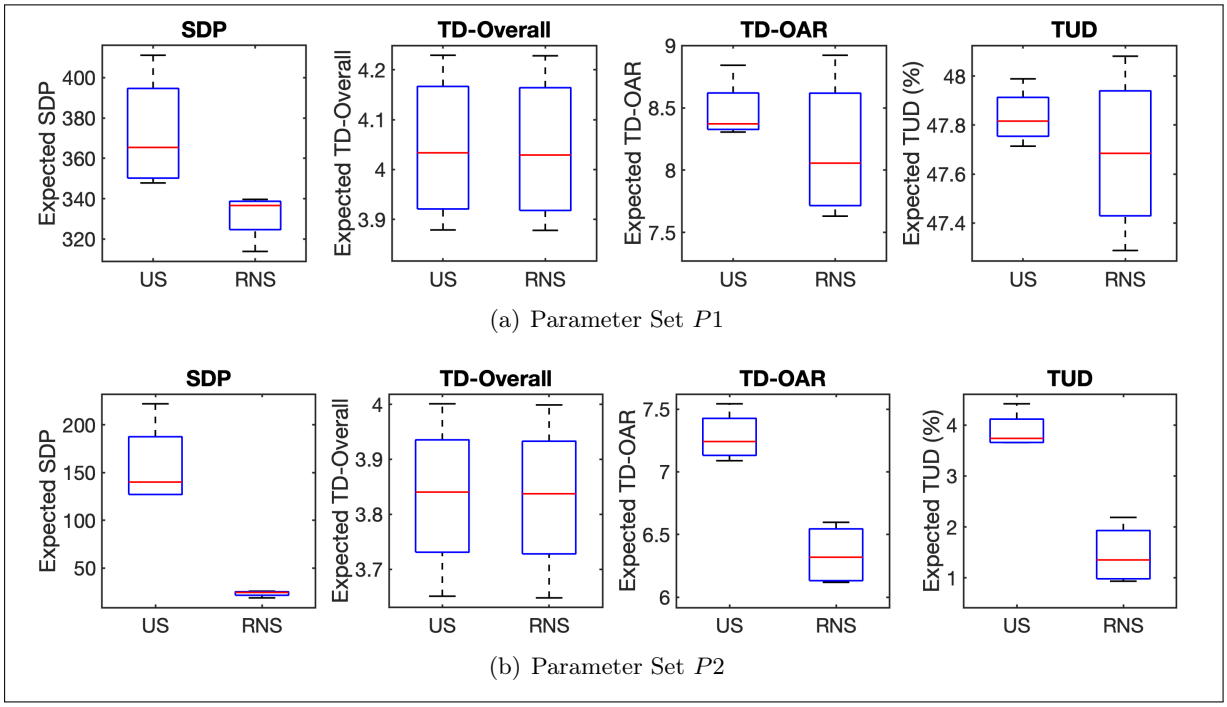

(a) Parameter Set $P1$

(b) Parameter Set $P2$

Figure 6: A Comprehensive Boxplot Comparison of Metrics of Interest for Stochastic Multistage Models under Parameter Sets $P1$ and $P2$.

fractionation schemes are not distinguishable in terms TD-Overall under both settings. There is a noticeable increase in the variance of TD-OAR and TUD metrics under $P1$ (observe the increased box widths). On the other hand, the domination of the nonuniform fractionation across all uncertainty representations is seen in the box plots associated with TD-OAR and TUD.

We further illustrate the differences between the uniform and nonuniform fractionation schemes by analyzing their performance across individual scenarios of a representative scenario tree, ST1. We begin by instantiating the multistage models for ST1, solve the resulting optimization problem to optimality, and compute the metrics of interest along each scenario of ST1. We present in Table 6 the results of this analysis for both parameter settings $P1$ and $P2$. For (**US**), the table shows the metrics for each of the four scenarios in ST1. On the other hand, for (**RNS**), the table shows the metrics along with the relative difference (in %) between the results obtained from (**RNS**) and (**US**). A positive (or a negative) difference indicates an improvement (or a deterioration) in performance from (**RNS**), when compared to (**US**). It is worthwhile to note that, as a consequence of observation in (7) and Proposition 4.1, the scenario-specific results for (**US**) in Table 6 are equivalent to the uniform deterministic fractionation (Procedure 1) applied to the corresponding scenario.

The results in Table 6 show that (**RNS**) dominates the uniform approach across all metrics for every realizable scenario under parameter set $P2$. However, this is not the case for the equally weighted setup of ($P1$). Table 6 reveals that although the uniform deterministic approach outperforms the nonuniform stochastic approach for certain scenarios (e.g., Scenario 3 for $P1$), it is impossible to identify such scenarios a priori. When (**US**) dominates (**RNS**), the magnitude tends to be less significant than when (**RNS**) outperforms (**US**). As is the case in comprehensive results (Table 5 and Figure 6), the advantages of nonuniform fractionation are more pronounced in setting $P2$, specifically with respect to metrics SDP, TD-OAR, and TUD. There is only marginal improvement in terms of TD-Overall.

Parameter Set $P1$					
	Scenario	SDP	TD-Overall	TD-OAR	TUD
(**US**)	1	462.8094	4.2105	8.4619	47.2232
	2	410.4636	3.9936	8.0620	48.8396
	3	345.8717	3.7215	8.5621	46.8360
	4	293.5260	3.5914	8.1370	48.4524
(**RNS**)	1	407.3993 (11.97%)	4.2084 (0.05%)	8.4942 (−0.38%)	47.0804 (0.30%)
	2	272.1991 (33.69%)	3.9936 (0.00%)	7.9351 (1.57%)	48.6540 (0.38%)
	3	355.5262 (−2.79%)	3.7183 (0.08%)	8.7129 (−1.76%)	46.4871 (0.75%)
	4	220.3260 (24.94%)	3.5901 (0.04%)	8.1116 (0.31%)	48.0606 (0.81%)
Parameter Set $P2$					
	Scenario	SDP	TD-Overall	TD-OAR	TUD
(**US**)	1	248.6650	3.9054	7.9473	4.9415
	2	247.5025	3.6895	7.5614	4.2037
	3	58.5761	3.5777	7.5132	3.4274
	4	57.4136	3.4314	7.1494	2.6896
(**RNS**)	1	24.0225 (90.34%)	3.9009 (0.11%)	6.3303 (20.35%)	1.6219 (67.18%)
	2	14.6681 (94.07%)	3.6864 (0.08%)	6.7227 (11.09%)	0.7182 (82.91%)
	3	22.7265 (61.20%)	3.5755 (0.06%)	5.4679 (27.22%)	1.3414 (60.86%)
	4	13.3720 (76.71%)	3.4302 (0.04%)	5.9519 (16.75%)	0.4378 (83.72%)

Table 6: An Illustrative Comparison of Metrics of Interest for Stochastic Multistage Models Across Each Individual Scenario of Scenario Tree ST1 under Parameter Sets $P1$ and $P2$.

4.3.2 An Illustrative Examination of DVHs under Stochastic Models

To provide an illustrative comparison to complement the scenario-based results in Table 6, we generate the DVHs corresponding to Scenario 2 of ST1 across both parameter sets $P1$ and $P2$. Here, Scenario 2 was chosen with the intention of providing DVHs that demonstrate conclusive takeaways in regards to the comparison between (**US**) and (**RNS**). However, as demonstrated in Table 6, Scenario 2 under $P1$ represents negligible differences between the performance of (**US**) and (**RNS**) across all four metrics. When Scenario 2 is considered under $P2$, the results in Table 6 give (**RNS**) a convincing advantage over (**US**). Collectively, the illustrative DVH comparisons align with the numerical output corresponding to Scenario 2 in Table 6.

The numerical results summarized in Table 6 along with the DVHs in Figures 7 and 8 also

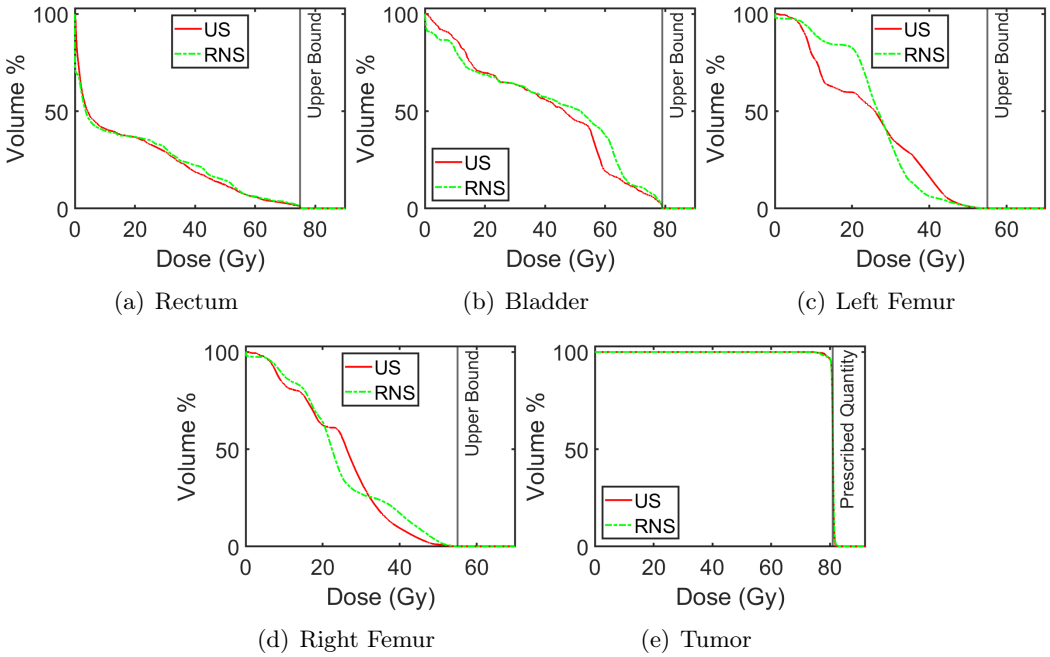

(a) Rectum (b) Bladder (c) Left Femur

(d) Right Femur (e) Tumor

Figure 7: An Illustrative Comparison of OAR and Prostate Tumor DVHs for Stochastic Multi-stage Models under Scenario 2 (Scans 2,1,3) of Scenario Tree ST1 and Parameter Set $P1$.

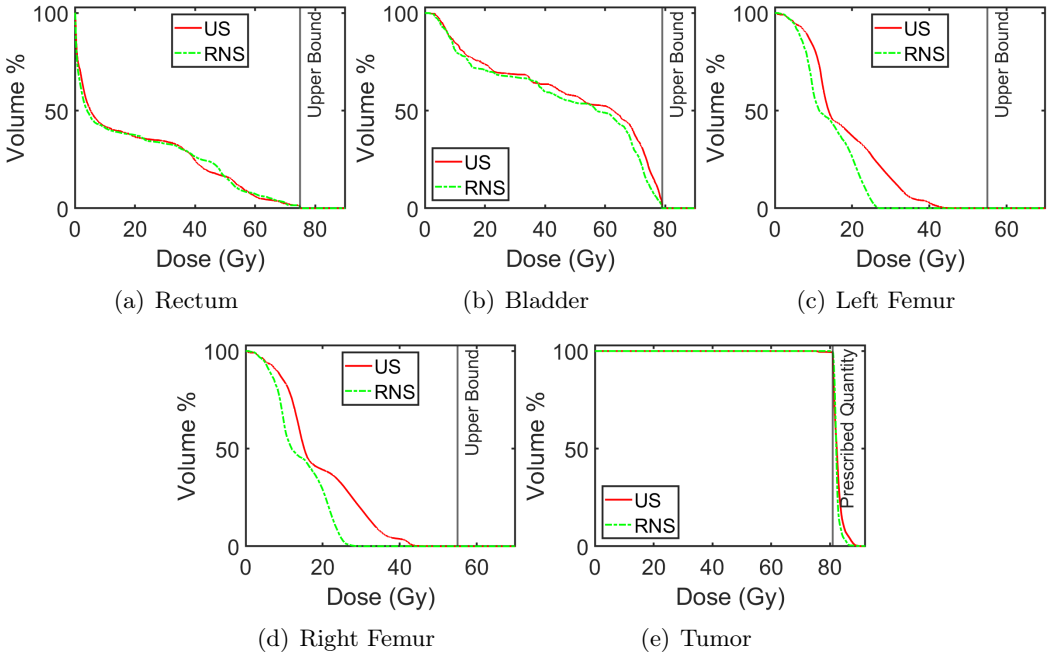

(a) Rectum (b) Bladder (c) Left Femur

(d) Right Femur (e) Tumor

Figure 8: An Illustrative Comparison of OAR and Prostate Tumor DVHs for Stochastic Multi-stage Models under Scenario 2 (Scans 2,1,3) of Scenario Tree ST1 and Parameter Set $P2$.

illustrate and support the necessity to consider nonuniform fractionation schemes in a stochastic problem setting. Although (**US**) is dominated in performance when compared with (**RNS**) under $P2$, both of these approaches are capable of providing valuable advantages over models which ignore uncertainty completely.

5 Conclusion

With advancements in radiation delivery technology and increased patient CT scan accessibility, optimization-based RTP practices have the opportunity and necessity to improve. The commonly practiced uniform fractionation approach to RTP allocates the same prescription dose limits and delivers radiation according to a specific FM in all treatment fractions. This approach cannot accommodate lookahead information or use predictive analytics tools to assess tumor evolution for planning. In an attempt to inform the current practice, we propose new modeling approaches that enable a superior representation of the multistage RTP problems by explicitly incorporating uncertainty.

Our proposed models simultaneously determine the dose prescription and FMs for all fractions. These models utilize lookahead information explicitly, and therefore, the resulting dose prescriptions and FMs adapt to the interfractional evolution of the patient's state. The stochastic variants of our proposed multistage models consider uncertainty in the future evolution of tumors to identify the treatment plan. We demonstrate that our proposed models can drastically improve the quality of treatment plans in terms of multiple metrics of interest. The improvements are maintained even when we restrict the underlying fractionation scheme to small intervals of nonuniformity. Hence, we argue that leveraging the stochastic programming methodology, accompanied with well-developed future patient CT scan predictions, has significant promise as a resource for RTP.

With technological and computational advancements, we expect that the multistage stochastic programming methodologies will continue to serve as resourceful optimization tools for RTP applications. Practitioners and cancer patients in the future will hopefully benefit from the utilization of these resources. Hence, further exploration of applying stochastic programming methodologies powered by predictive analytics tools to design effective RTP practices under uncertainty remains a fruitful research direction.

References

[1] P. M. Pardalos and H. E. Romeijn. *Handbook of Optimization in Medicine*. Springer Science & Business Media, 2009.

[2] A. Holder and B. Salter. A tutorial on radiation oncology and optimization. In *Tutorials on Emerging Methodologies and Applications in Operations Research*, pages 4:1–4:47. Springer, 2005.

[3] R. Baskar, K. A. Lee, R. Yeo, and K-W. Yeoh. Cancer and radiation therapy: Current advances and future directions. *International Journal of Medical Sciences*, 9(3):193–199, 2012.

[4] M. D. Mills and S. Y. Woo. History of IMRT. In *Intensity-Modulated Radiation Therapy*, pages 3–14. Springer, 2015.

[5] B. S. Teh, S. Y. Woo, and E. B. Butler. Intensity modulated radiation therapy (IMRT): A new promising technology in radiation oncology. *The Oncologist*, 4(6):433–442, 1999.

[6] T. Bortfeld. Optimized planning using physical objectives and constraints. In *Seminars in Radiation Oncology*, volume 9, pages 20–34. Elsevier, 1999.

[7] T. Bortfeld. IMRT: A review and preview. *Physics in Medicine & Biology*, 51(13):R363–R379, 2006.

[8] A. Brahme, J-E Roos, and I. Lax. Solution of an integral equation encountered in rotation therapy. *Physics in Medicine & Biology*, 27(10):1221–1229, 1982.

[9] M. Ehrgott, Ç. Güler, H. W. Hamacher, and L. Shao. Mathematical optimization in intensity modulated radiation therapy. *Annals of Operations Research*, 175(1):309–365, 2010.

[10] A.T. Redpath, B.L. Vickery, and D.H. Wright. A new technique for radiotherapy planning using quadratic programming. *Physics in Medicine & Biology*, 21(5):781–791, 1976.

[11] S. C. McDonald and P. Rubin. Optimization of external beam radiation therapy. *International Journal of Radiation Oncology - Biology - Physics*, 2(3-4):307–317, 1977.

[12] L. K. Mell, J. C. Roeske, and A. J. Mundt. A survey of intensity-modulated radiation therapy use in the united states. *Cancer*, 98(1):204–211, 2003.

[13] D. M. Shepard, M. C. Ferris, G. H. Olivera, and T. R. Mackie. Optimizing the delivery of radiation therapy to cancer patients. *Siam Review*, 41(4):721–744, 1999.

[14] G. Starkschall. A constrained least-squares optimization method for external beam radiation therapy treatment planning. *Medical Physics*, 11(5):659–665, 1984.

[15] S. Webb. The physical basis of IMRT and inverse planning. *The British journal of radiology*, 76(910):678–689, 2003.

[16] H. E. Romeijn and J. F. Dempsey. Intensity modulated radiation therapy treatment plan optimization. *TOP*, 16(2):215–243, 2008.

[17] C. Men, H. E. Romeijn, A. Saito, and J. F. Dempsey. An efficient approach to incorporating interfraction motion in IMRT treatment planning. *Computers & Operations Research*, 39(7):1779–1789, 2012.

[18] W. Lu, M. Chen, Q. Chen, K. Ruchala, and G. Olivera. Adaptive fractionation therapy: I. basic concept and strategy. *Physics in Medicine & Biology*, 53(19):5495–5511, 2008.

[19] M. C. Ferris and M. M. Voelker. Fractionation in radiation treatment planning. *Mathematical Programming*, 101(2):387–413, 2004.

[20] J. Ramakrishnan, D. Craft, T. Bortfeld, and J. N. Tsitsiklis. A dynamic programming approach to adaptive fractionation. *Physics in Medicine and Biology*, 57(5):1203–1216, 2012.

[21] A. Ghate. Dynamic optimization in radiotherapy. In *INFORMS TutORials in Operations Research: Transforming Research into Action*, pages 60–74. INFORMS, 2011.

[22] R.E. Drzymala, R. Mohan, L. Brewster, J. Chu, M. Goitein, W. Harms, and M. Urie. Dose-volume histograms. *International Journal of Radiation Oncology - Biology - Physics*, 21(1):71–78, 1991.

[23] F. Saberian, A. Ghate, and M. Kim. Spatiotemporally optimal fractionation in radiotherapy. *INFORMS Journal on Computing*, 29(3):422–437, 2017.

[24] D. Yan, F. Vicini, J. Wong, and A. Martinez. Adaptive radiation therapy. *Physics in Medicine & Biology*, 42(1):123–132, 1997.

[25] F. Saberian, A. Ghate, and M. Kim. Optimal fractionation in radiotherapy with multiple normal tissues. *Mathematical Medicine and Biology: A Journal of the IMA*, 33(2):211–252, 2016.

[26] F. Saberian and M. Kim. Phantom creator (phanc): A matlab software for creating phantom test cases for IMRT optimization, working draft of the user's manual. *University of Washington*, 2014.

[27] T. Bortfeld, W. Neve, R. Schmidt-Ullrich, and D. E. Wazer. *Image-Guided IMRT*. Springer, 2006.

[28] D. Yan and D. Lockman. Organ/patient geometric variation in external beam radiotherapy and its effects. *Medical Physics*, 28(4):593–602, 2001.

[29] E. Rietzel, G. T.Y. Chen, N. C. Choi, and C. G. Willet. Four-dimensional image-based treatment planning: Target volume segmentation and dose calculation in the presence of respiratory motion. *International Journal of Radiation Oncology - Biology - Physics*, 61(5):1535–1550, 2005.

[30] M. Chu, Y. Zinchenko, S. G. Henderson, and M. B. Sharpe. Robust optimization for intensity modulated radiation therapy treatment planning under uncertainty. *Physics in Medicine & Biology*, 50(23):5463–5477, 2005.

[31] T. C.Y. Chan, T. Bortfeld, and J. N. Tsitsiklis. A robust approach to IMRT optimization. *Physics in Medicine & Biology*, 51(10):2567–2583, 2006.

[32] J. Unkelbach, M. Alber, M. Bangert, R. Bokrantz, T. C.Y. Chan, J. O. Deasy, A. Fredriksson, B. L. Gorissen, M. Van Herk, W. Liu, et al. Robust radiotherapy planning. *Physics in Medicine & Biology*, 63(22):22TR02:1–28, 2018.

[33] G. J. Lim, L. Kardar, S. Ebrahimi, and W. Cao. A risk-based modeling approach for radiation therapy treatment planning under tumor shrinkage uncertainty. *European Journal of Operational Research*, 280(1):266–278, 2020.

[34] M. Zaghian, G. J. Lim, and A. Khabazian. A chance-constrained programming framework to handle uncertainties in radiation therapy treatment planning. *European Journal of Operational Research*, 266(2):736–745, 2018.

[35] Y. An, J. Liang, S. E. Schild, M. Bues, and W. Liu. Robust treatment planning with conditional value at risk chance constraints in intensity-modulated proton therapy. *Medical Physics*, 44(1):28–36, 2017.

[36] M. Y. Sir, M. A. Epelman, and S. M. Pollock. Stochastic programming for off-line adaptive radiotherapy. *Annals of Operations Research*, 196(1):767–797, 2012.

[37] A. Shapiro, D. Dentcheva, and A. Ruszczynski. *Lectures on Stochastic Programming: Modeling and Theory*. SIAM, 2014.

[38] J. R. Birge and F. Louveaux. *Introduction to Stochastic Programming*. Springer, 2011.

A Appendix: Summary of Essential Notation

Sets	
N	Total number of fractions in the radiation treatment plan
$\mathcal{T}$	Set of all relevant patient structures
$\mathcal{O}$	Set of organs-at-risk (OAR)
$\mathcal{V}_n^{(i)}$	Set of all voxels v belonging to structure i during fraction n
$\mathcal{B}$	Set of all radiation beamlets
$\mathcal{K}$	Set of all possible scenarios corresponding to a scenario tree
$\mathcal{J}$	Set of all nodes corresponding to a scenario tree
τ	Upper-bound quantity imposed on aggregate dose (AD)
Parameters	
ξ	Observation of the stochastic process $\tilde{\xi}$ capturing interfractional uncertainty
L^{tumor}	Total prescribed tumor dosage (in Gy units)
$\mathbf{u}$	Universal upper bounds for each OAR (in Gy units)
ϵ	Parameter describing freedom of nonuniformity ($\epsilon \in [0, M]$)
$\mathbf{A}_n$	Dose-deposition matrix ($\lvert\mathcal{V}_n\rvert \times \lvert\mathcal{B}\rvert$) in fraction n
(w_n^+, w_n^-)	Scalar importance weights characterizing tumor dosing preferences
$p_n^{(j)}$	Probability of visiting node j during fraction n
$P1$	Parameter set with equal weights, i.e., $w_n^+ = w_n^- = 0.5$, for all fractions n
$P2$	Parameter set with weights $w_n^+ = 0.001, w_n^- = 0.999$ for all fractions n
Decision Variables	
$z_n^{(i)}$	Upper bound dosage for all voxels belonging to OAR i during fraction n
ℓ_n	Prescribed tumor dosage for fraction n
x_{vn}	Dosage given to voxel v during fraction n
y_{bn}	Intensity of beamlet b during fraction n